Development of Field Modulation in a Split-Field Drift Tube for High-Throughput Multidimensional Separations

Stormy L. Koeniger, Stephen J. Valentine, Sunnie Myung, Manolo Plasencia, Young Jin Lee,[†] and David E. Clemmer*

Department of Chemistry, Indiana University, Bloomington, Indiana 47405

A field modulation approach for high-throughput ion mobility/time-of-flight analyses of complex mixtures has been developed using a split-field drift tube. In this approach, complex mixtures of peptides, such as those that arise from tryptic digestion of protein mixtures, are separated by nanocolumn liquid chromatography, ionized by electrospray ionization, and analyzed by ion mobility/time-of-flight techniques. The split-field drift tube allows parent ions to be separated based on differences in their low-field mobilities through the first-field region before entering the second region. For increased throughput, the magnitude of the field in the second region can be modulated throughout an LC separation in order to favor transmission of different types of ions: parent ions at low fields; fragments from primarily $[M+3H]^{3+}$ peptides at moderate fields; or, fragmentation of $[M+3H]^{3+}$ and $[M+2H]^{2+}$ species at higher fields. We demonstrate the approach with two examples: a mixture of tryptic peptides from digestion of hemoglobin; and a complex mixture of tryptic peptides from digestion of human plasma.

Keywords: ion mobility • drift tube • collision induced dissociation • high-field fragmentation

Introduction

The emerging field of proteomics has been driven by spectacular advances in analytical instrumentation. Methods that utilize two-dimensional gel electrophoresis[1,2] (and in some cases, additional gel separation dimensions) and mass spectrometry (MS) strategies for identification are now widely applied.[3–9] Additionally, many approaches for coupling multiple dimensions of liquid chromatography (LC) separations with MS (in an on-line fashion) have also emerged.[10–14]

Although strategies for proteome analysis now exist, the development of new technologies remains a central barrier for addressing systems of enormous complexity. Few approaches are capable of determining a global proteomic map with enough resolution, sensitivity, and reproducibility, to allow direct comparisons of all components between proteomes to be made. Arguably two-dimensional (2D) gel approaches of intact proteins provide the best strategy for total proteome display; however, these approaches are time and labor intensive, and it is difficult to reproducibly display proteins in identical positions from run-to-run and lab-to-lab. Hyphenated LC–MS and LC–MS/MS strategies, such as those used in commercial instruments, are typically designed for analysis of peptides obtained from digest mixtures of proteins. These methods aim to find and identify as many of the largest peaks within complex mixtures as possible—not to provide a reliable measure and identification of all components present in complex mixtures. As sample complexity increases back-to-back LC–MS/MS scans often do not identify the same components (even for replicate analyses of the same sample). At least in part, these systems are limited by the initial selection of a single m/z ion for subsequent fragmentation. As ions are selected for short times in order to carry out MS/MS studies, the mixture composition that is eluting from the column changes; thus, it is difficult to retain enough information to reliably identify peaks for all components present for a global comparison between experiments.

During the past few years, we have attempted to address some of these issues by introducing a fast gas-phase separation based on the mobilities of ions through a buffer gas, ion mobility spectrometry (IMS).[15,16] In this approach, ions are pulsed into a drift tube containing a buffer gas and are subjected to a weak electric field. Ions are dispersed according to differences in their average collision cross section and charge states. Upon exiting the drift tube, the mobility-dispersed ions can be introduced into a time-of-flight mass spectrometer (TOF–MS) for mass analysis; or, they may be subjected to energizing collisions that generate fragment ions (and then subsequently mass analyzed). In the latter case, fragment ions, formed by collision-induced dissociation (CID) after the mobility separation, can be grouped together based on the coincidence in drift times of species that arise from common precursors. With this approach, it is possible to rapidly record fragmentation patterns for multiple ions in parallel.[17–19]

Parallel fragmentation after a drift tube has been accomplished with several techniques which include fragmenta-

tion in an octopole collision cell,[17] with an orifice-skimmer cone,[18] by surface-induced-dissociation (SID),[20] and more recently with a high field located at the back of a split-field drift tube.[19] Prior to the development of a split-field drift tube, the ability to obtain sequential parent (MS) and fragmentation information (CID−MS) during a single LC separation was problematic due to the changes in instrument conditions between the MS and CID−MS modes of operation. The split-field drift tube design has the advantage of being able to obtain MS and CID−MS information within seconds by simply changing the magnitude of the second field. In addition, the ability to separate and dissociate ions inside the drift tube substantially simplifies the design of the instrument described here, relative to other instruments.

In this paper, we demonstrate that the magnitude of the electric field in the second-field region of the drift tube can be modulated on-line so that it is possible to obtain MS and CID−MS spectra (for all species that are present) in a single LC−IMS−TOF experiment. We demonstrate this with a simple tryptic digest mixture of human hemoglobin. Overall, the approach provides a rapid means of characterizing complex mixtures and the mobility separation reduces spectral congestion, making it possible to detect low-abundance components even when more abundant species are present. Although the method of separating and dissociating ions in a drift tube using two field regions is relatively new, the approach is simple to implement. Data acquired with the field modulation approach for the analysis of a human plasma sample is presented.

Experimental Section

General Experimental Approach. The fundamental principles and applications of IMS techniques[21] as well as the overall instrument design housing the split-field drift tube[19] have been presented previously. A detailed description of the modifications made for modulation experiments and a brief description of the experimental approach are presented here. Briefly, the experimental approach of LC−IMS−MS and LC−IMS−CID−MS is as follows. A mixture of tryptic peptides is separated on a pulled-tip, packed capillary column by reversed-phase LC (discussed in detail below). As the peptides elute from the column, they are ionized by electrospray ionization (ESI)[1] and extracted into a differentially pumped region of the vacuum system. The continuous beam of ions that is produced enters the main vacuum chamber ($\sim3 \times 10^{-4}$ Torr) and is accumulated in a linear geometry octopole ion trap. Ion mobility separations are initiated with a pulse of the accumulated ion packet into the entrance of a split-field drift tube[19] containing He buffer gas. Ions are separated based on the differences in their low-field mobilities across the first-field region (operated at 5 V cm^{-1}) of the drift tube. Near the end of the drift tube, ions pass through a wire grid and enter a second-field region that can be operated at low fields in order to transmit parent ions, or substantially higher fields in order to collisionally activate parent ions and form fragment ions. Under the latter conditions, the total drift times of all of the ion fragments that are generated from dissociation of a single parent are coincident, creating an effective label that can be used to group fragments and parent ions together. The overall approach allows CID−MS experiments to be carried out on a mixture of ions in parallel as reported previously.[17]

Ions exit the drift tube through a differentially pumped orifice skimmer cone region (used previously in CID−MS experiments)[18] and are extracted into a high-vacuum chamber ($\sim2 \times 10^{-6}$ Torr) where they are collimated and focused into the source region of a reflectron geometry TOF−MS. Here, the ions are extracted orthogonally into the flight tube where they are dispersed based on their m/z ratios. Due to differences in the time scales of the LC (min), IMS (ms), and TOF−MS (μs) separations, it is possible to record data in a *nested* fashion, as described previously;[15,16] $\sim10^2$ to 10^3 TOF spectra can be recorded in the time required to record a single ion-mobility distribution; $\sim10^5$ to 10^6 ion-mobility distributions can be recorded over the total time required for the LC separation. It is convenient to report peptide retention times (t_R), ion drift times (t_D), and ion flight times (t_F) in a fashion that reflects the measurement; here, we report times as $t_R[t_D(t_F)]$ in units of min[ms(μs)] or values of LC-frame number[ms(m/z)].

Preparation of Tryptic Peptide Mixtures. A simple mixture of tryptic peptides from a single protein (human hemoglobin, Sigma 95%) was generated by digestion with 2% (w/w) trypsin (TPCK-treated bovine pancrease, Sigma) in a solution containing 0.2 M tris(hydroxymethyl)aminomethane buffer (pH 8.0) and 2 M urea at 37 °C for 24 h. Prior to analysis, the peptides were purified with microconcentrators (Microcon 10, Amicon, Inc.) having a 10 000 MW cutoff and with Sep-Pak C$_{18}$ (Waters) sample extraction cartridges to remove digest reagents. The resulting peptide solution was lyophilized and stored at −80 °C.

A more complicated tryptic peptide mixture was obtained from digestion of a human plasma sample. The following procedure was used to work up the sample prior to injection into the instrument. A 1.0 mL aliquot of the plasma sample was dissolved in phosphate buffered saline (PBS) solution (pH = 7.5) containing urea (8 M). Disulfide bonds were reduced and alkylated by addition of dithiothreitol (10 mM; incubated at 37 °C for 2 h) and then iodoacetamide (20 mM; incubated in darkness at 0° for 2 h). The reaction was quenched by adding cysteine. The protein solution was diluted to a final urea concentration of 2 M, digested by adding 2% (w/w) TPCK-treated trypsin, and then incubated at 37 °C for 24 h. Tryptic peptides were purified with Oasis HLB cartridges, lyophilized, and stored at −80 °C.

LC Separation and Ion Formation. The nanospray separation system consists of a 10-port valve, an 1100 series Cap LC (Agilent, Palo Alto, CA), a nanocolumn (75 μm ID × 150 mm), and a trapping column (100 μm ID × 15 mm) flowing at 250 nL/min. The fused-silica nanocolumn and trapping column are packed with a methanol slurry of 5 μm, 100 Å Magic C18AQ and 200 Å Magic C18 (Microm BioResourses Inc., Auburn, CA), respectively. The trapping column and nanocolumn are coupled through a PEEK microcross in which the trapping column is located immediately before the nanocolumn. The third connection to the microcross, perpendicular to the flow, contains a platinum wire used to apply an electrospray voltage of 2 kV. Prior to LC separation, the sample is preconcentrated by injection of the tryptic digest (50 ng of hemoglobin peptides and 800 ng of plasma peptides) onto the trapping column for 8−10 min with 100% solvent A (3% acetonitrile in water and 0.1% formic acid) and 0% solvent B (acetonitrile with 0.1% formic acid). Chromatographic separation is achieved over a $\sim20−30$ min linear-gradient program. Additional details of the separation system have been described previously.[22]

Linear Ion Trap and Split-Field Drift Tube. A detailed schematic of the linear ion trap and split-field drift tube is shown in Figure 1. Improvements in sensitivity by replacement of a Paul trap[23] with a linear ion trap (LIT) have been reported
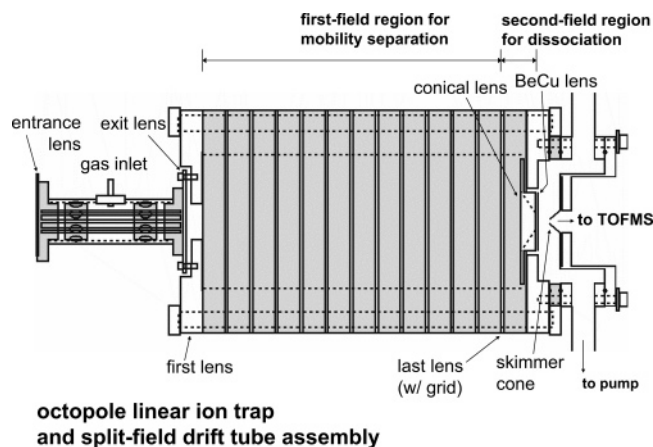
Figure 1. Detailed schematic of the split-field drift tube and linear octopole trap. The potentials modulated for precursor ion and fragment ion analysis include the first (drift-tube) lens, the last lens with grid, and the conical lens.

previously.[24] The octopole trap is 8.0 cm long and is constructed with 8 stainless steel rods (3.2 mm DIA) positioned with $r_0 =$ 2.9 mm by two Macor mounting pieces housed within a stainless steel case. Assuming that the field is ideal within the ion cloud radius, we estimate the upper-limit charge capacity to be $\sim$2 × 10^{10} e.[25] Confinement of the ions axially within the trap occurs by applying appropriate dc potentials to two end caps (0.7-mm-thick stainless steel plates with entrance and exit apertures of $\sim$3 mm each) of the LIT. An rf generator (built in-house) supplies a potential of 800 V_{p-p} with a dc bias of $\sim$35 V relative to the drift voltage and a 1.1-MHz frequency to the octopole rods. Ions are injected directly into the drift tube at a frequency of 167 Hz by dropping the potential applied to the exit end cap by $\sim$20 V for a period of 100 μs. For the current configuration, the injection time is limited to 100 μs and cannot be decreased without the loss of high m/z ions. However, this injection time is still much lower than the millisecond time scale of the mobility separation and does not affect the resolution. Multiple trapping conditions have been optimized for a range of injection energies into the drift tube as well as for various systems including proteins[26] and peptides.

The split-field drift tube comprises two independent field regions and has a total length of 21.9 cm with 1.0 mm diameter entrance and exit apertures. The drift tube is operated at $\sim$1.7 Torr, as measured with a capacitance manometer (model 640A Baratron, MKS). Mobility separations occur in the first region ($\sim$20 cm) of the drift tube between the first (drift tube) lens and the last lens (see Figure 1). Twelve equally spaced 0.16-cm-thick, stainless steel rings separated with 1.27-cm-thick Delrin spacers are connected in series with 100-MΩ high-vacuum resistors (K and M Electronics, Inc., ± 1%) to create the uniform electric field ($\sim$5 V·cm^{-1}) in the first region. A short region ($\sim$1.90 cm) of the drift tube between the last lens containing a Ni mesh grid (90% transmittance, Buckbee-Mears, St. Paul, MN) and the BeCu lens is operated under nonlinear fields created by a combination of potentials applied to the last lens, conical lens, and BeCu lens. When the second region of the drift tube is operated in the low-field regime, parent ion m/z ratios are measured. As the field in this region is increased, the high-field[27] regime is reached, and ions can undergo energetic collisions that lead to dissociation. The potential used to obtain parent ion data is 55 V and the fragment ion data is obtained with 220 V. This potential is applied to both the last
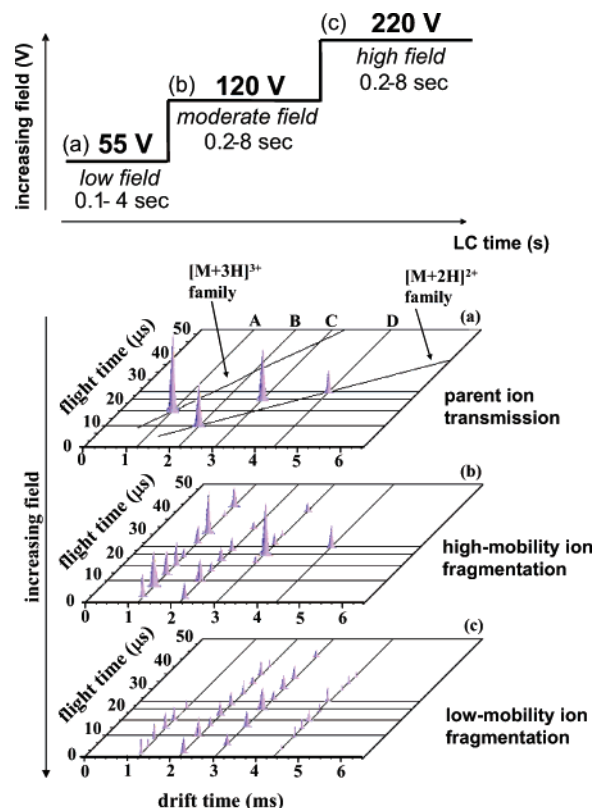
Figure 2. Field modulation cycle for a sequence of potentials applied to the split-field drift tube and the corresponding hypothetical $t_D(t_F)$ datasets are shown. The potentials shown represent those applied to both the drift tube last lens and the conical lens (see Figure 1). A low field is applied to transmit parent ions (a) through the second field region, while higher fields are applied to produce mobility-labeled fragments of high-mobility ions (b) and low-mobility ions (c).

lens and the conical lens (Figure 1). To increase extraction efficiency, the conical lens potential is set 1 V less than the (drift tube) last lens. The potentials reported in the following discussions will refer to the potential applied to the last lens. Under these conditions, the resolving power of the drift tube [$t_D/\Delta t_{D(fwhm)}$] is $\sim$15 for most singly charged ions and as high as 35 for multiply charged ions.[28] In addition to the new region at the back of the drift tube, a differentially pumped region located between the BeCu lens and the skimmer cone (see Figure 1) is also used to increase ion-extraction efficiency.[18] Orifice skimmer cone (OSC) dissociation utilized previously in parallel sequencing[18] is minimized by application of a low-potential difference ($\sim$0.5 to 2 V) between the BeCu plate and the skimmer cone.

Field Modulation within a Split-Field Drift Tube. Parent ion and fragmentation spectra can be obtained sequentially by modulation of the potentials applied to the second region of the drift tube. Cycling between MS and CID−MS modes of operation is performed with three fast, high-voltage operational amplifiers (APEX Microtechnology Corp.) that are controlled by a computer program designed within our data acquisition system. Each high-voltage amplifier supplies the varying potentials to the drift tube entrance plate, last lens, and conical lens (See Figure 1). Data acquisition software queries the user for the number of different potentials to be utilized in an experiment as well as the duration of each potential. An illustration of the field modulation utilized in the experiments
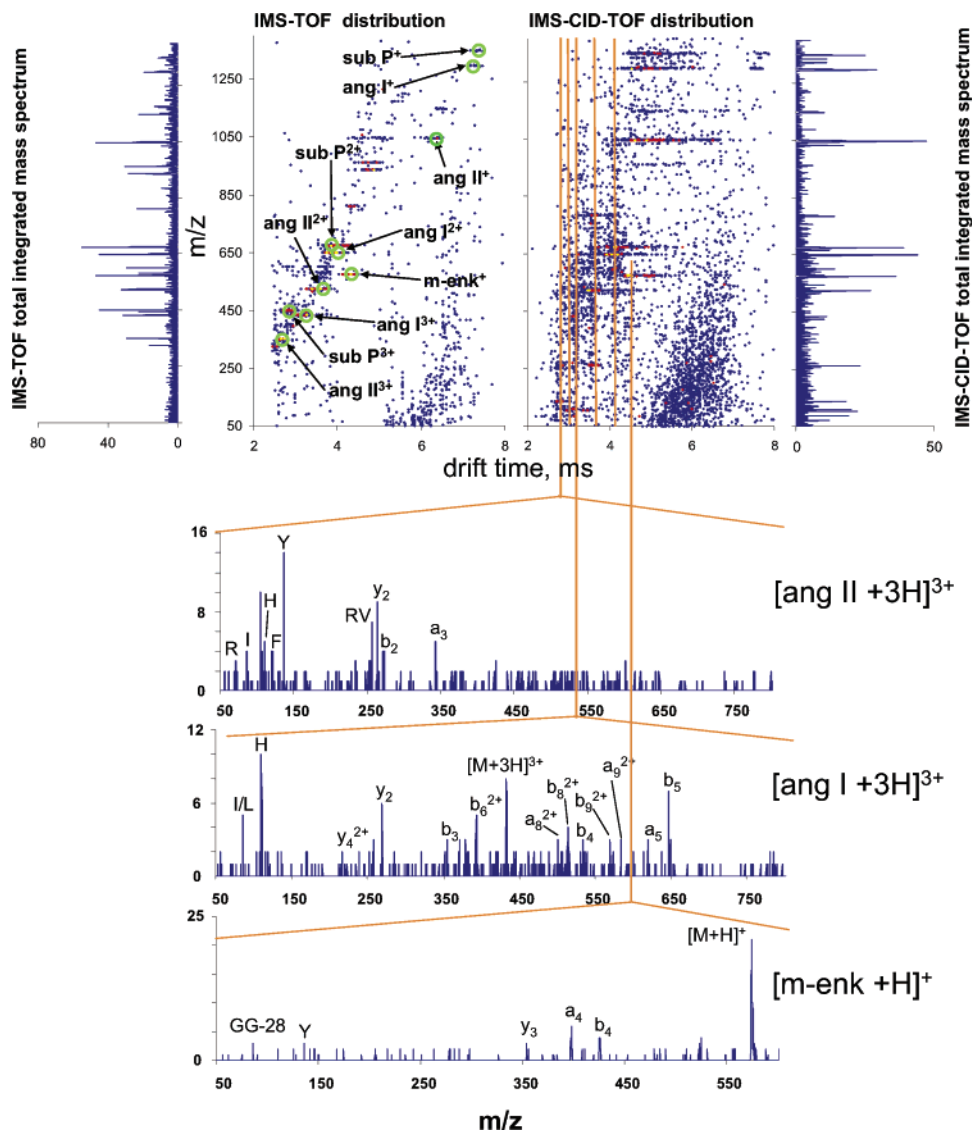
Figure 3. (top) Nested drift(flight) time, $t_D(t_F)$, distributions (center) and integrated mass spectra (sides) for an electrosprayed mixture of methionine enkephalin (m-enk), angiotensin II, angiotensin I, and substance P obtained for 100 ms (10 experimental scans). Peptides were electrosprayed from a 1 mg ml^{-1} (0.25 mg mL^{-1} of each peptide) solution containing 49:49:2 (%volume) of water/acetonitrile/ acetic acid. The distribution on the left was obtained in precursor ion mode without argon gas in the octopole collision cell. The distribution on the right was obtained under CID conditions (addition of 1.8×10^{-4} Torr argon to the octopole collision cell). Mass spectral slices of the data are obtained by integrating over small drift time ranges. Six vertical lines on the top right distribution indicate CID−MS spectra for [M+3H]$^{3+}$ of angiotensin II, substance P, and angiotensin I, [M+2H]$^{2+}$ of angiotensin II, angiotensin I, and substance P, and [M+H]$^{1+}$ of m-enk (from left to right). CID−MS spectra for [M+2H]$^{2+}$ of angiotensin I and substance P are not separable.). (bottom) The CID−MS spectra obtained for drift times centered at 2.8, 3.2, and 4.5 ms are shown for [M+3H]$^{3+}$ of angiotensin II and angiotensin I and [M+H]$^{1+}$ of m-enk.

reported here for obtaining parent ions at 55 V (a), low-field fragmentation at 120 V (b), and high-field fragmentation at 220 V (c) is shown at the top of Figure 2. Hypothetical IMS−TOF distributions corresponding to this field modulation cycle are shown in Figure 2 to illustrate the transmission of parent ions (a), fragmentation of high-mobility ions (b), and fragmentation of low-mobility ions (c) observed in typical modulated experiments. Note the difference in fragmentation efficiency (hypothetical) at moderate fields (b) and high fields (c) between peptide ions A and B versus C and D. These potentials are chosen empirically by optimizing the fragmentation of the [M+3H]$^{3+}$ and [M+2H]$^{2+}$ of bradykinin (98% purity, Sigma) electrosprayed from a solution of 2.4×10^{-2} M in 49:49:2 (% volume) water:acetonitrile:acetic:acid. All experiments reported

here maintain a field of ∼5 V·cm^{-1} across the first region of the drift tube to minimize differences in drift times between MS and CID−MS modes.

Acquisition of $t_R[t_D(t_F)]$ Datasets. As discussed above, the centroid of a peak can be defined in three-dimensional space by $t_R[t_D(t_F)]$. For the studies presented here, the retention time, drift time, and flight time ranges recorded are between ∼4 to 34 min, ∼1 to 6 ms, and ∼9.7 to 38.0 μs, respectively. It is straightforward to carry out longer LC separations−gradients extending over 5 h have been used. Flight times are converted to m/z values from a calibration of a known mixture, and typically we focus the analysis over a m/z range of ∼155−2000. Retention times are calculated from timing parameters described as follows: after an initial delay of 4 min from the start
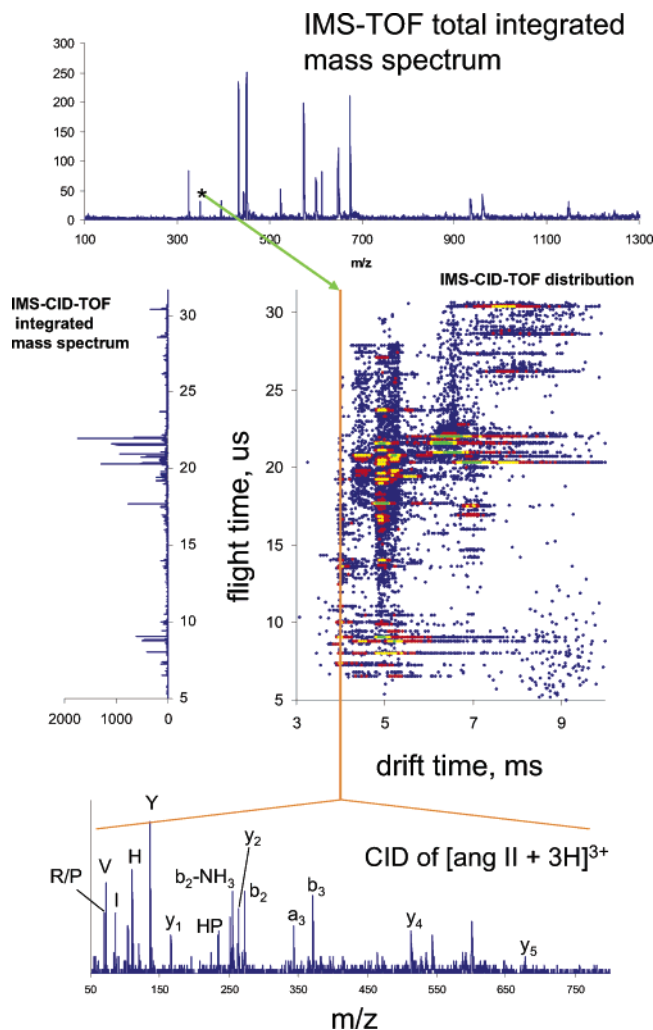
Figure 4. Parent ion peak for [M+3H]$^{3+}$ of angiotensin II in the total mass spectrum (top) is marked with an asterisk to indicate its low abundance in a mixture containing four peptides [70 μg/mL for angiotensin I, substance P, Met-enkephalin and 7 μg/mL for angiotensin II in H$_2$O:acetonitrile:acetic acid = 49:49:2 (%volume)]. The parallel fragmentation of these components is shown in the $t_D(t_F)$ distribution (center) with the total integrated mass spectrum (left). A CID mass spectrum of the low abundance ion (t_D = 3.8 ms) is obtained by integration over a narrow drift time range (bottom).

of the LC gradient, 300 nested $t_D(t_F)$ datasets, acquired for 6 s each, are recorded sequentially. Each $t_D(t_F)$ dataset is referenced from the start of the acquisition by a frame number; thus, the retention time can be determined from the equation: t_R = initial delay from start of gradient + (frame number × acquisition time per frame). Recent advances in our acquisition system allow LC frames to be acquired in real time (no dead time from saving each dataset); this is an improvement over our previous system, which required up to 3.0 s for saving each frame.[16]

Data acquisition for field modulated experiments is performed as before, however the acquisition time per frame can be varied for each potential allowing shorter acquisition times for MS and longer acquisition times for CID−MS. Data presented for the single digest were acquired for 4 s (55 V), 8 s (120 V), and 8 s (220 V) resulting in a total modulation-cycle time of 20 s; elution time of a single LC-separated ion in this study is on the order of 40−60 s which allows 2−3 complete modulation cycles of MS and CID−MS data to be recorded for
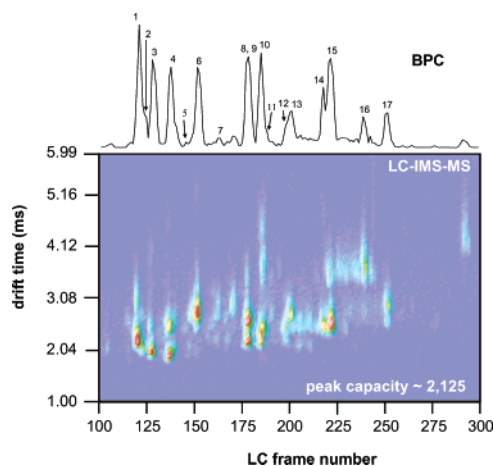
Figure 5. A LC−IMS−TOF contour plot of a hemoglobin digest (50 ng). Each frame (a nested drift(flight) time distribution) represents 6 s of consecutive acquisition during a LC separation. The base peak chromatogram is shown with labeled peak numbers corresponding to the identified components in the mixture (Table 1). From this contour plot, parent ion mass spectra are obtained by integration of each spot across LC frames (retention times) and drift times. A nonlinear color scale is used.

each peptide. The time scheme used in these experiments allows 660 mobility distributions to be summed at 55 V and 1330 distributions at 120 and 220 V for each cycle. Modulation of the potentials applied to the drift tube is controlled in parallel with the collection of a single frame; thus, frames representing each potential can be extracted from the set of frames recorded for the entire LC separation. For example, in a three step modulation cycle, every third frame, starting with the first frame, can be extracted to create an LC−IMS−MS dataset representing all the parent ions obtained at 55 V; likewise, every third frame, starting with the second or third frame, can be extracted to create an LC−IMS−CID−MS dataset representing the fragmentation at 120 or 220 V, respectively. Because, 2−3 complete cycles of MS and CID−MS data can be obtained during the elution of a single peak, frames corresponding to the same potential for the same ion can be summed for higher intensity spectra.

Results and Discussion

Example of Fast CID. As a demonstration of fast acquisition of MS and CID−MS information consider the data shown in Figure 3. This figure shows nested IMS−TOF and IMS−CID−TOF distributions recorded for a well-defined mixture of small peptide ions (see figure for details). In the IMS−CID−TOF distribution, parent ions were separated in the drift tube, extracted into a vacuum chamber, and then accelerated at a desired kinetic energy through an octopole collision cell. This distribution was recorded in 10 experimental cycles (a total time of 100 ms) and it is possible to observe fragment ions from six different parents during this time. Example CID−MS spectra for three parent ions (angiotensin I, angiotensin II, and methionine enkephalin) obtained by integration of the data across drift time regions specific for these ions are shown at the bottom of the figure. The ability to generate fragments for individual parents for a mixture of six ions in 100 ms demonstrates the potential utility of this approach as a high-speed device for characterizing peptides. We note that while in some cases the peaks shown are near the signal-to-noise (S/N) ratios

Table 1. Summary of Assigned Parent Ions for a Human Hemoglobin Tryptic Digest

peak[a]	$t_R[t_D(m/z)]$[b]	m/z_{calc}	sequence[c]	position (chain)
1	16.0[2.87(766.0)]	765.82	[VGAHAGEYGAEALER+2H]$^{2+}$	17−31 (α)
	16.0[2.16(510.8)]	510.88	[VGAHAGEYGAEALER+3H]$^{3+}$	
2	16.4[2.54(575.8)]	575.68	[VVAGVANALAHK+2H]$^{2+}$	133−144 (β)
	16.4[1.96(384.2)]	384.12	[VVAGVANALAHK+3H]$^{3+}$	
3	16.7[3.75(819.5)]	818.95	[VDPVNFK+1H]$^{1+}$	93−99(α)
	16.7[1.92(409.8)]	409.97	[VDPVNFK+2H]$^{2+}$	
4	17.7[2.41(564.9)]	564.12	[LHVDPENFR+2H]$^{2+}$	96−104 (β)
	17.7[1.92(376.4)]	376.41	[LHVDPENFR+3H]$^{3+}$	
5	18.5[2.66(690.7)]	690.28	[EFTPPVQAAYQK+2H]$^{2+}$	121−132 (β)
6	19.1[2.66(658.5)]	658.21	[VNVDEVGGEALGR+2H]$^{2+}$	18−30 (β)
7	20.3[2.87(787.94)]	786.93	[FLASVSTVLTSKYR+2H]$^{2+}$	128−141 (α)
8	21.8[3.33(918.1)]	918.01	[TYFPHFDLSHGSAQVK+2H]$^{2+}$	41−56 (α)
	21.8[2.46(612.4)]	612.34	[TYFPHFDLSHGSAQVK+3H]$^{3+}$	
	21.8[2.21(459.6)]	459.51	[TYFPHFDLSHGSAQVK+4H]$^{4+}$	
9	21.8[2.37(573.35)]	574.37	[LLGNVLVCVLAHHFGK+3H]$^{3+}$	105−120 (β)
10	22.5[4.16(933.1)]	933.09	[SAVTALWGK+1H]$^{1+}$	9−17 (β)
	22.5[2.21(467.1)]	467.05	[SAVTALWGK+2H]$^{2+}$	
11	23.1[2.75(711.92)]	711.8	[GTFATLSELHCDK+2H]$^{2+}$	83−95 (β)
12	23.9[2.41(544.6)]	544.65	[LRVDPVNFK+2H]$^{2+}$	91−99 (α)
13	24.1[2.71(627.6)]	627.24	[FLASVSTVLTSK+2H]$^{2+}$	128−139 (α)
14	25.8[4.58(1072.5)]	1072.31	[MFLSFPTTK+1H]$^{1+}$	32−40 (α)
	25.8[2.46(536.8)]	536.65	[MFLSFPTTK+2H]$^{2+}$	
15	26.2[3.33(836.1)]	835.95	[VLGAFSDGLAHLDNLK+2H]$^{2+}$	67−82 (β)
	26.2[2.50(557.7)]	557.64	[VLGAFSDGLAHLDNLK+3H]$^{3+}$	
16	27.9[3.50(1030.0)]	1030.64	[FFESFGDLSTPDAVMGNPK+2H]$^{2+}$	41−59 (β)
	27.9[2.71(687.6)]	687.43	[FFESFGDLSTPDAVMGNPK+3H]$^{3+}$	
17	29.2[3.33(1001.28)]	1000.11	[VADALTNAVAHVDDMPNALSALSDLHAHK+3H]$^{3+}$	62−90 (α)
	29.2[2.79(750.7)]	750.33	[VADALTNAVAHVDDMPNALSALSDLHAHK+4H]$^{4+}$	

^{a} Peak number corresponds to the elution order in the chromatographic separation. ^{b} Parent ion experimental retention time, drift time, and m/z in units of min, ms, and Da, respectively. ^{c} Assignment of tryptic peptide ion. Note in all cases assignments are made from parent ion m/z values (measured at low fields) and assignments are corroborated by fragmentation patterns (obtained at high fields).

for detection, these assignments are confirmed in datasets obtained using longer acquisition times.

A second advantage of the IMS−CID−TOF approach is illustrated in Figure 4. This system is the same as that shown in Figure 3; however, the concentration of one of the peptides (angiotensin II) has been reduced to 10% of the concentration of the others. This is reflected in the peak height of the +3 charge state as indicated in the figure. The IMS−CID−TOF spectrum (and integrated CID−MS spectrum) demonstrates that it is possible to record fragmentation patterns for low-abundance ions in the presence of more abundant species. This may become especially important for complex systems of unknown peptides such as those often encountered in proteomics studies; as, it is non trivial to select low-abundance peptide ions for MS/MS studies in the presence of higher-abundance components in standard on-line LC−MS and LC−MS/MS studies.

Analysis of a Single Protein Digest Using a Split-Field Drift Tube. For purposes of development, in early experiments, we often recorded LC−IMS−MS and LC−IMS−CID−MS information in two separate runs. It is useful to examine these data. Figure 5 shows a two-dimensional $t_R(t_D)$ contour plot representing a three-dimensional $t_R[t_D(t_F)]$ dataset of the parent ion data for a hemoglobin digest; the fragment ion contour plot is not shown to minimize redundancy. The contour plot is obtained by integration of ion intensities over all flight times (t_F) at each drift time (t_D) for all LC frames. Above the contour plot is the base peak chromatogram (BPC) for the parent ion data. Seventeen tryptic peptides having between 7 and 29 amino acids were identified out of 23 expected tryptic peptides with ≥4 amino acids. Of the six peptides not observed in LC−IMS−TOF only three including LLSHCLLVTLAAHLPAEFT-PAVHASLDK, LLVVYPWTQR, and AAWGK were observed via direct infusion of the sample. The three peptides not observed

in either direct infusion or LC−IMS−TOF were the TNVK, AHGK, and GHGK sequences, all four residues long. These peptides may not have been observed in the LC−IMS−TOF approach because they eluted from the column prior to data acquisition, or perhaps because they are not ionized efficiently in the LC experiment -presumably they elute from higher aqueous concentrations. The larger peptides, having a large number of relatively hydrophobic amino acids, may not be observed because they bind irreversibly to the column or have poor ionization efficiencies.

Table 1 provides a comparison of theoretical and experimental m/z values that are used to assign peptides.[29] Further confirmation of parent ion assignments can be obtained by examining the fragmentation patterns produced in the second region of the drift tube.[30] Multiple charge states, including [M+H]$^+$ to [M+4H]$^{4+}$, are observed for many of the peptides throughout the LC separation. Typically doubly charged ions are the most abundant. Analysis of typical peak widths across the LC and IMS separation dimensions provide an estimate of the 2D LC−IMS peak capacity. Prior to m/z analysis, peak capacities range from ∼2000 to 3000 for short LC separation times (i.e., 20 min); higher values can be obtained with longer LC separation times. The peak capacity in the data shown is estimated to be ∼2100.

On-Line Field Modulation Experiments of a Single Protein Digest. Figure 6 shows three two-dimensional $t_R(t_D)$ contour plots obtained from one LC separation using the voltages and time durations described above in the field modulation cycle. Each contour plot is shown on an identical nonlinear color scale and frame numbers correspond to 20 s of LC separation time. The parent ion contour plot (a) is created from extracted nested datasets in the LC run under parent ion conditions where the potential applied to the last lens was 55 V (as explained above). Although the duty cycle for the parent ion
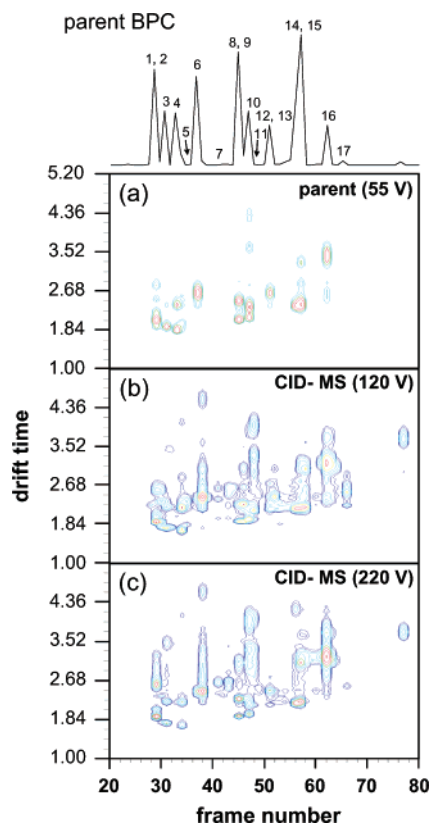
Figure 6. Contour plots of a single LC−IMS−TOF analysis of hemoglobin digest (50 ng). The three datasets labeled parent (55 V), CID−MS (120 V), and CID−MS (220 V) are obtained with the modulation cycle shown in Figure 2. Tryptic peptide identifications are indicated on the base peak chromatogram (top). Each contour plot is shown on an identical nonlinear color scale. See text for details.

mode in this experimental sequence is only 20%, all 17 ions identified above with 100% duty cycle were observed. The fragment ion contour plots labeled b and c are created from extracted nested datasets where the applied potential was 120 and 220 V, respectively. The base peak chromatogram for the parent ion data is at the top. Interestingly, for the CID−MS datasets, several lower-mobility species are observed that were not observed in the parent ion dataset. Typically, these features correspond to singly charged peptides. One possibility for the inability to see these features in the parent ion plot is that the nonlinear field in the second region of the drift tube is weak immediately after the last lens such that these low-mobility, low-intensity species are not extracted efficiently from the drift tube and are not observed because they fall below the detection limit of the measurement.

Figure 7 shows three $t_D(t_F)$ datasets in which two modulation cycles were summed for each potential to enhance the signal-to-noise (S/N) ratios. During the first (left dataset) potential step (55 V) of the field-modulation cycle, the $[M+2H]^{2+}$ and $[M+3H]^{3+}$ ions of the peptide VGAHAGEYGAEALER are observed. When the voltage is increased to 120 V (middle dataset) fragmentation of the $[M+3H]^{3+}$ ion is observed while the parent $[M+2H]^{2+}$ ion persists. Increasing the last lens potential further to 220 V (right dataset), increased fragmentation efficiency of the $[M+3H]^{3+}$ ion as well as fragmentation of the $[M+2H]^{2+}$ ion is observed. Mass spectral slices obtained by integration of a narrow drift time range are shown for [VGAHAGEYG-AEALER+3H]$^{3+}$ (top) and [VGAHAGEYGAEALER+2H]$^{2+}$ (bot-

tom) at the three potentials. Fragment ions produced from the doubly- and triply charged ions are mostly y- and b-type ions. Internal fragments, not previously observed, are obtained at high potentials for the $[M+3H]^{3+}$ ion. Shifts in the drift time between parent ion and fragment ion conditions, caused by the increase in the extraction fields at the back of the drift tube, are readily calibrated to maintain the mobility label of the parent. The shift in drift times between 50 and 120 V applied to the last lens is significant (in most cases <0.3 ms). This shift is less significant upon changing from 120 to 220 V. The shifts that are observed appear to be both charge state and analyte dependent. Although calibration of these shifts allows the data to be interpreted at this point, we are currently exploring this effect in more detail as it is likely that information about the analyte may be discernible.

As with other CID methods, fragmentation efficiency of the high-field fragmentation method is dependent on the size and charge state of the parent ion. Voltage settings that are too low will not induce fragmentation of some ions while it has been observed that many smaller, highly charged ions as well as their fragments are lost if the voltage settings are too high. Although not unambiguous, the loss of small (and high charge state) ions at the highest fields appears to come about because primary and secondary fragments continue to undergo fragmentation and thus, only very small charged species are left for m/z analysis. Additional fragmentation can also increase or decrease the distribution of fragment ions observed. Overall, modulation of the second-field region in order to acquire significant fragmentation information over a range of conditions is advantageous for sequence identification in a mixture containing a broad range of different peptide lengths and charge states.

Example of Field Modulation in a More Complex Mixture: Tryptic Peptides from Human Plasma. As a developmental milestone, it is important to show the extension of this approach to a more complex sample of biological importance. We have chosen to show preliminary data for analysis of peptides from digestion of proteins extracted from human plasma. The aim of showing these data is to empirically demonstrate the developmental state of the instrumentation and modulated approach. At their current state of development, it is not possible to provide a detailed analysis of the data, because the software for interpreting these data is still under development.

Examples of modulated data from peptides obtained by digesting proteins from plasma are shown in Figure 8. Here, four representative nested $t_D(t_F)$ distributions that were obtained with the last lens potential set at 60 (recorded for 4s), 200 (3s), 265 (3s), and 310 V (3s). In this experiment, ~800 ng of sample was separated by LC (as described above) using a fast gradient in which solvent B was increased from 10 to 38% over 21 min in three steps. The first $t_D(t_F)$ distribution (using 60 V for the second-field region) was initiated at a retention time of 16.83 min. This distribution is dominated by a complex distribution of tryptic peptide parent ions. These ions fall into charge state families (as described previously). Upon increasing the second-field voltage to 200 V, we observe that many of the peptides undergo substantial fragmentation. In particular relatively low molecular weight +3 peptides (with high mobilities) that appear at short drift times (~4 to 6.5 ms) undergo extensive dissociation. At higher voltages (265 and 310 V) the distribution of m/z values associated with these higher mobility ions is shifted to lower m/z values—indicating that the initial fragments continue to dissociate. In addition, we observe
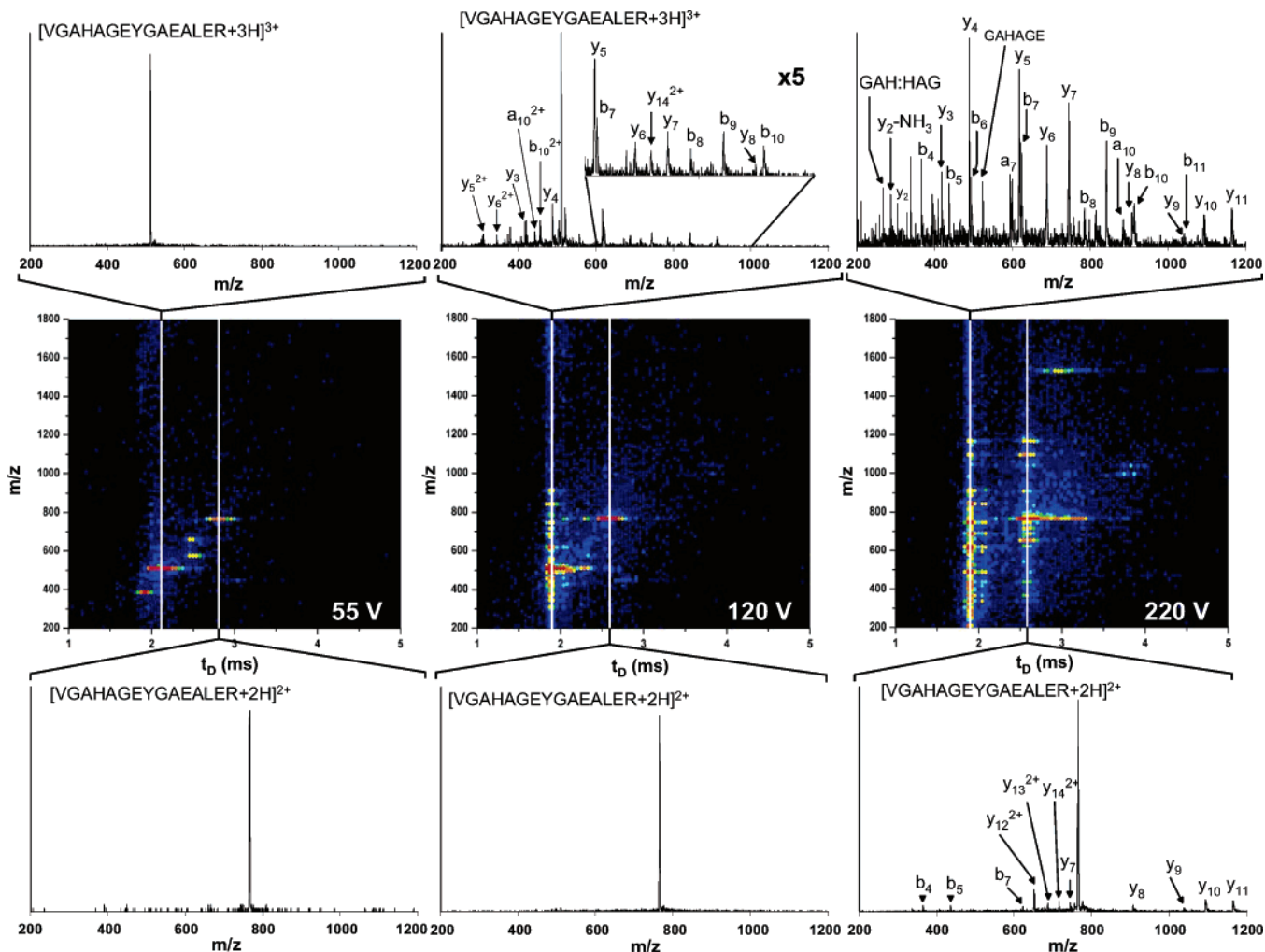
Figure 7. LC−IMS−MS and LC−IMS−CID−MS data obtained sequentially during the modulation of the field in the second region of the drift tube. (middle) Nested drift(flight) time distributions showing the parent and fragmentation of the peptide sequence VGAHAGEYGAEALER at 55, 120, and 220 V as indicated. Mass spectral slices for the corresponding potentials are shown for the [M+3H]$^{3+}$ (top) and [M+2H]$^{2+}$(bottom) of VGAHAGEYGAEALER.

substantial fragmentation of other peptides that were not dissociated at low fields (60 or 200 V).

It is interesting to consider the types of peptide ions that dominate these distributions. Figure 9 shows several mass spectral slices taken through the 310 V plot of Figure 8. We have analyzed these data by comparing the combined data from the measured parent ion masses from the 60 V data (in this case measured m/z values of 411.36, 671.98, and 737.89) with the fragment ion data shown in Figure 9 and values from the Swiss−Prot[31] database through a MASCOT[32] search. This search indicates highly probable assignments of these peptides as: the QGLLPVLESFK peptide (ion score = 51 from MASCOT) from the Apolipoprotein A-1 protein; the AVMDDFAAFVEK sequence (ion score = 68 from MASCOT) of Serum Albumin; and, the ATLVCLISDFYPGAVTVAWK peptide (ion score = 57 from MASCOT) from the Immunoglobulin λ Chain (C region) protein. Two of these assignments (the QGLLPVLESFK and AVMDDFAAFVEK sequences) were also made from the data recorded at second-field voltages of 200 and 265 V; however, the ATLVCLISDFYPGAVTVAWK peptide was only observed under the most energetic conditions; this illustrates the utility of modulating the field over a range of fragmentation conditions.

A final point about this system involves the assignments that are made. These assignments are satisfying based not only on the scores that were obtained but also from consideration that these proteins are all known to be among the most abundant proteins found in plasma.[33] Many other peptides from these proteins are observed at other retention times. Interestingly, even though peptides from abundant proteins are found across the entire experiment; these features often are found at slightly different retention times and drift times. Thus, our preliminary analysis indicates that many additional peptides from low-abundance proteins can also be identified. We are currently in the process of developing software that will be used to analyze these datasets in more detail and will describe the approach in more detail elsewhere.[34]

Qualitative Assessment of Reproducibility Associated with Complex Mixture Analysis: Comparison with Scanning Techniques. An important feature of the LC−IMS−MS approaches that we have described is that each of these separation dimensions involves dispersive rather than scanning techniques. As noted in the Introduction, scanning devices (e.g., quadrupoles) may not select the same parent ions from run to run (even for the same sample) because of slight shifts in the relative parent ion abundances. This lack of reproducibility for
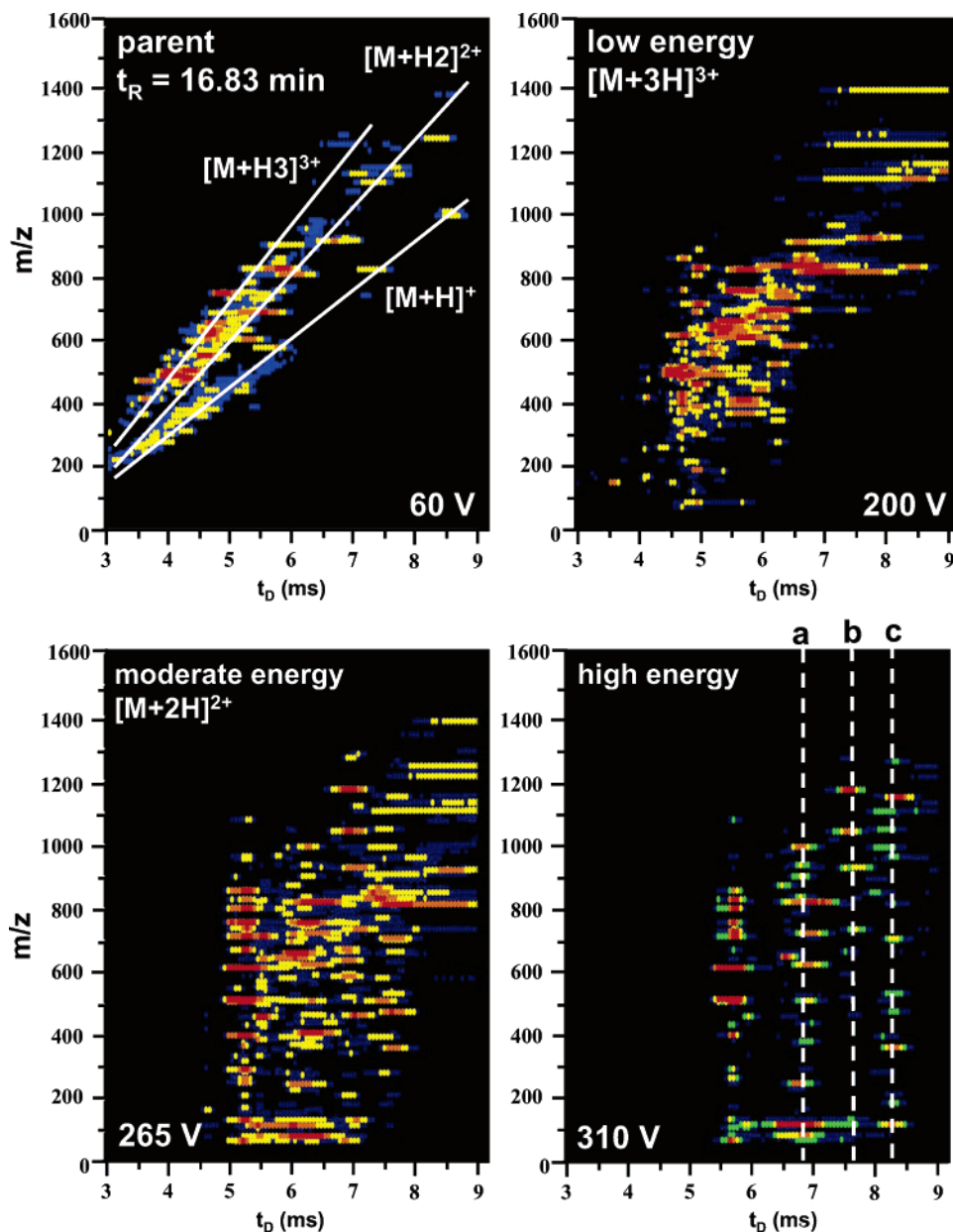
Figure 8. Four nested $t_D(t_F)$ datasets of an on-line field modulation analysis of a tryptic digest of plasma are shown. All four datasets represent a total of 13 s of LC separation time (60 V for 4 s, 200 V for 3 s, 265 V for 3 s, and 310 V for 3 s). The potentials applied to the last lens are indicated on the corresponding dataset and dashed lines labeled a–c on the 310 V dataset indicate the location of the CID–MS data shown in Figure 9.

scanning devices increases in significance as the number of components in the sample goes up. Similar changes in relative ion abundances are also encountered in the LC–IMS–(CID)–MS approach. However, because no initial parent ion m/z selection is employed the run-to-run reproducibility is not influenced by the initial ion selection. For a prepared digest of a single commercially available protein, we find that ion intensities (for parent peptide ions) typically vary over a range of ±10 to ±30%. Even for very complex samples, such as the mixture of peptides from digestion of proteins from plasma (Figure 8), overlaying datasets shows evidence for essentially all peaks above a defined threshold in both the LC–IMS–TOF and LC–IMS–CID–TOF modulated spectra (from run to run). This comparison is best done by visual inspection of the data sets. Our early attempts to automate peak identification (i.e.,

find the positions and intensities of all resolved features, and create files that can be used for MASCOT type searches) also show that run-to-run reproducibility for which parent and fragment ions are present (in the modulated dataset) appears to be higher than the reproducibility for scanning instruments. For these comparisons the reproducibility of the LC-Q analysis is lower in the sense that several runs are required to converge upon the number of peptides that can be identified with this approach. Having said this, we note that the ability to identify peptides (from run-to-run) for the same sample from LC–IMS–MS methods is still highly limited because of limitations in software. Although the measurement reproducibility with LC–IMS–MS is high the reproducibility in the number of peptide assignments that can be made in an automated fashion is relatively low. We are currently testing several approaches for
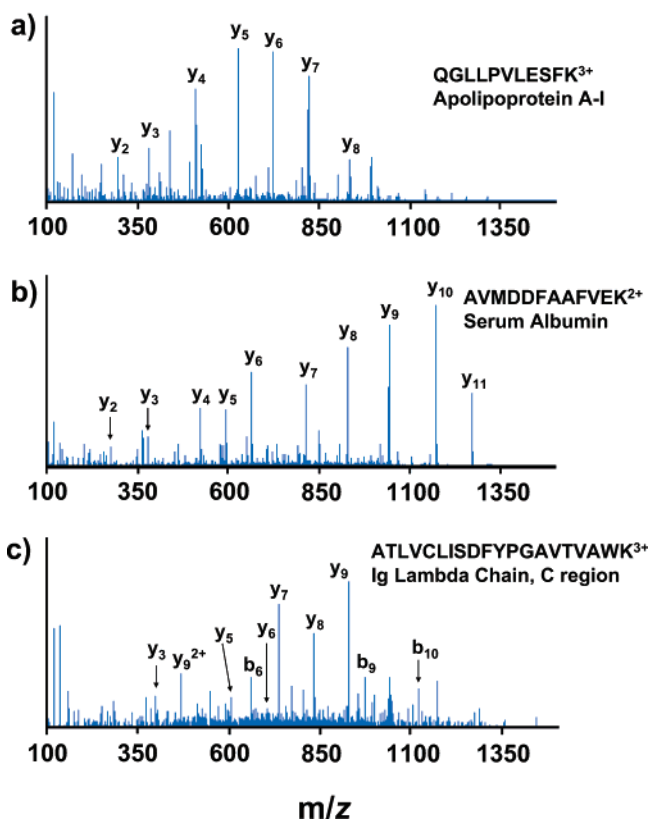
Figure 9. Fragmentation mass spectra obtained at high field conditions in which a voltage of 310 V was applied to the last lens (see Figure 1). The CID−MS spectra correspond to (a) the QGLLPVLESFK peptide from the Apolipoprotein A-1 protein; (b) the AVMDDFAAFVEK sequence of Serum Albumin; and, (c) the ATLVCLISDFYPGAVTVAWK peptide from the Immunoglobulin λ Chain (C region) protein. Efficient fragmentation was also observed for the sequences QGLLPVLESFK and AVMDDFAAFVEK at second-field voltages of 200 and 265 V.

automation and will report a detailed assessment in future work. Finally, in a sense, the modulated approach presented here is a scanning method, especially when several drift field fragmentation conditions are used. We do not currently anticipate using more than ∼10 unique conditions (within the second field region) with this type of modulation cycle (i.e., a 10% duty cycle for any single condition).

Conclusions and Outlook

A field modulation approach utilized for acquiring parent and fragment ion information during an LC−IMS−TOF separation has been demonstrated by examining a simple mixture of tryptic peptides obtained from digestion of human hemoglobin and compared to a standard method of analysis. The approach incorporates a split-field drift tube design in which the magnitude of the second-field region can be modulated over short time scales (∼0.1 to 10 s). The field modulation technique offers several advantages over previous methods, which require two LC−IMS−TOF experiments to obtain both MS and CID−MS information. The sequential acquisition of MS and CID−MS spectra eliminates the need to align parent and fragmentation datasets acquired with two separate LC separations. For proteomic and complex mixture analyses, field modulation has significantly increased the throughput of this technology as well as simplified LC−IMS−TOF data analysis programs.

A particularly attractive feature of the present instrumental design is its simplicity. The ability to separate and induce fragmentation in a second-field region within the drift tube makes it possible to eliminate an additional collision cell (and all of the ion optics associated with focusing in to and out of the collision cell that we previously reported).[18] Additionally, field modulation appears to be a simple means of providing substantial control over the type of fragmentation that is observed. That is, it is possible to tune conditions such that virtually no fragmentation occurs (parent ion conditions) or, favor fragmentation of some types of ions. For example, we showed that it is possible to selectively fragment $[M+3H]^{3+}$ ions while inducing very minimal fragmentation in $[M+2H]^{2+}$ species. The selectivity of the fragmentation at high pressures may arise because the collisional excitation initiates from a population of thermalized ions and the activation process is averaged over many collisions. Because of this, the impact parameter associated with the initial collision should be relatively unimportant in the fragmentation process.

In the configuration described here, we activate ions in a nonuniform field (a balloon shaped field that is also used to focus ions out of the exit orifice of the drift tube); we anticipate that tighter control of the fragmentation process may be obtained by modulation of a uniform field. We are currently developing a split-field instrument with two linear fields in order to examine this in more detail. This should also allow us to examine two additional issues that arose during this study: sampling differences, primarily involving low-mobility ions that appear to be focused more effectively at higher fields; and, slight differences in drift times that arise because of the different residence times associated with the second-field region (at different fields).

References

(1) O'Farrell, P. H. *J. Biol. Chem.* **1975**, *250*, 4007−4021.
(2) Klose, J. *Humangenetik* **1975**, *26*, 231−244.
(3) Shevchenko, A.; Jensen, O. N.; Podtelejnikov, A. V.; Sagliocco, F.; Wilm, M.; Vorm, O.; Mortensen, P.; Shevchenko, A.; Boucherie, H.; Mann, M. *P. Natl. Acad. Sci. U.S.A.* **1996**, *93*, 14440−14445.
(4) Rabilloud, T. *Proteomics* **2002**, *2*, 3−10.
(5) Cordwell, S. J.; Nouwens, A. S.; Verrills, N. M.; Basseal, D. J.; Walsh, B. J. *Electrophoresis* **2000**, *21*, 1094−1103.
(6) Franzen, B.; Becker, S.; Mikkola, R.; Tidblad, K.; Tjernberg, A.; Birnbaum, S. *Electrophoresis* **1999**, *20*, 790−797.
(7) Lim, S. O.; Park, S. J.; Kim, W.; Park, S. G.; Kim, H. J.; Kim, Y. I.; Sohn, T. S.; Noh, J. H.; Jung, G. *Biochem. Bioph. Res. Comm.* **2002**, *291*, 1031−1037.
(8) Sinha, P.; Hutter, G.; Kottgen, E.; Dietel, M.; Schadendorf, D.; Lage, H. *J. Biochem. Biophys. Methods* **1998**, *37*, 105−116.
(9) Gygi, S. P.; Rochon, Y.; Franza, B. R.; Aebersold, R. *Mol. Cell. Biol.* **1999**, *19*, 1720−1730.
(10) Spahr, C. S.; Davis, M. T.; McGinley, M. D.; Robinson J. H.; Bures, E. J.; Beierle, J.; Mort, J.; Courchesne, P. L.; Chen, K.; Wahl, R. C.; Yu, W.; Luethy, R.; Patterson, S. D. *Proteomics* **2001**, *1*, 93−107.
(11) Link, A. J.; Eng, J.; Schieltz, D. M.; Carmack, E.; Mize, G. J.; Morris, D. R.; Garvik, B. M.; Yates, J. R. *Nat. Biotechnol.* **1999**, *17*, 676−682.
(12) Ducret, A.; Van Oostveen, I.; Eng, J. K.; Yates, J. R.; Aebersold, R. *Protein Sci.* **1998**, *7*, 706−719.

(13) Jensen, P. K.; Pasa-Tolic, L.; Peden, K. K.; Martinovic, S.; Lipton, M. S.; Anderson, G. A.; Tolic, N.; Wong, K. K.; Smith, R. D. *Electrophoresis* **2000**, *21*, 1372−1380.

(14) Lubman, D. M.; Kachman, M. T.; Wang, H.; Gong, S.; Yan, F.; Hamler, R. L.; O'Neil, K. A.; Zhu, K.; Buchanan, N. S.; Barder, T. J. *J. Chromatogr. B* **2002**, *782*, 183−196.

(15) Hoaglund, C. S.; Valentine, S. J.; Sporleder, C. R.; Reilly, J. P.; Clemmer, D. E. *Anal. Chem.* **1998**, *70*, 2236−2242. Henderson, S. C.; Valentine, S. J.; Counterman, A. E.; Clemmer, D. E. *Anal. Chem.* **1999**, *71*, 291−301. Hoaglund-Hyzer, C. S.; Clemmer, D. E. *Anal. Chem.* **2001**, *73*, 177−184.

(16) Valentine, S. J.; Kulchania, M.; Srebalus Barnes, C. A.; Clemmer, D. E. *Int. J. Mass Spectrom.* **2001**, *212*, 97−109. Srebalus Barnes, C. A.; Hilderbrand, A. E.; Valentine, S. J.; Clemmer, D. E. *Anal. Chem.* **2002**, *74*, 26−36. Lee, Y. J.; Hoaglund-Hyzer, C. S.; Srebalus Barnes, C. A.; Hilderbrand, A. E.; Valentine, S. J.; Clemmer, D. E. *J. Chromatography B* **2002**, *782*, 343−351.

(17) Hoaglund-Hyzer, C. S.; Li, J.; Clemmer, D. E. *Anal. Chem.* **2000**, *72*, 2737−2740.

(18) Lee, Y. J.; Hoaglund-Hyzer, C. S.; Taraszka, J. A.; Zientara, G. A.; Counterman, A. E.; Clemmer, D. E. *Anal. Chem.* **2001**, *73*, 3549−3555.

(19) Valentine, S. J.; Koeniger, S. L.; Clemmer, D. E. *Anal. Chem.* **2003**, *75*, 6202−6208.

(20) Stone, E. G.; Gillig, K. J.; Ruotolo, B. T.; Fuhrer, K.; Gonin, M.; Schultz, A.; Russell, D. H. *Anal. Chem.* **2001**, *73*, 2233−2238. Stone, E. G.; Gillig, K. J.; Ruotolo, B. T.; Russell, D. H. *Int. J. Mass Spectrom.* **2001**, *212*, 519−533.

(21) For general reviews, see the following and the references therein: St. Louis, R. H.; Hill, H. H., Jr. *Crit. Rev. Anal. Chem.* **1990**, *21*, 321; Clemmer, D. E.; Jarrold, M. F. *J. Mass Spectrom.* **1997**, *32*, 577−592; Ewing, R. G.; Atkinson, D. A.; Eiceman, G. A.; Ewing, G. J. *Talanta* **2001**, *54*, 515−529. Hilderbrand, A. E.; Valentine, S. J.; Clemmer, D. E. Mobilities: Biological Systems and Clusters In ***Encyclopedia of Mass Spectrometry*** *(Theory and Ion Chemistry, Volume 1)*; Gross, M. L., Caprioli, R., Armentrout, P., Eds.; Elsevier: Kidlington, Oxford, 2003; p 506−520. Wyttenbach, T.; Bowers, M. T. *Top. Curr. Chem.* **2003**, *225*, 207−232.

(22) Moon, M. H.; Myung, S.; Plasencia, M.; Hilderbrand, A. E.; Clemmer, D. E. *J. Proteome Res.* **2003**, *2*, 589−597.

(23) Hoaglund, C. S.; Valentine, S. J.; Clemmer, D. E. *Anal. Chem.* **1997**, *69*, 4156−4161.

(24) Myung, S.; Lee, Y. L.; Moon, M. H.; Taraszka, J. A.; Sowell, R.; Koeniger, S. L.; Hilderbrand A. E.; Valentine, S. J.; Cherbas, L.; Cherbas, P.; Kaufmann, T. C.; Miller, D. F.; Mechref, Y.; Novotny, M. V.; Ewing, M.; Clemmer, D. E. *Anal. Chem.* **2003**, *75*, 5137−5145.

(25) Tolmachev, A. V.; Udseth, H. R.; Smith, R. D. *Anal. Chem.* **2000**, *72*, 970−978.

(26) Sowell, R. A.; Koeniger, S. L.; Valentine, S. J.; Moon, M. H.; Clemmer, D. E. *J. Am. Soc. Mass Spectrom.* **2004**, *15*, 1341−1353.

(27) Mason, E. A.; McDaniel; E. W. *Transport Properties of Ions in Gases*; Wiley: New York, 1988.

(28) All of the plots in the present paper represent ion mobility distributions within a two-dimensional plot where the intensity is specified using a color gradient. With this type of plot we are often attempting to show very small peaks in the presence of large peaks. Therefore, large peaks extend over a much broader range of drift times because we are effectively showing the base width of the peak. A feeling about the shapes of ion distributions across the drift time distribution can be obtained by examining data in the references to other work.

(29) A list of peptides produced from tryptic digestion of human hemoglobin for up to three missed cleavages was produced from the web database PeptideMass (http://us.expasy.org/tools/peptide-mass.html).

(30) Fragment ion assignments were made by comparison of experimental m/z ratios with average *m/z* ratios obtained from the MS−Product program from Protein Prospector (http://prospector.ucsf.edu).

(31) Boeckmann, B.; Bairoch, A.; Apweiler, R.; Blatter, M.-C.; Estreicher, A.; Gasteiger, E.; Martin, M. J.; Michoud, K.; O'Donovan, C.; Phan, I.; Pilbout, S.; Schneider, M. *Nucleic Acids Res.* **2003**, *31*, 365−370. Apweiler, R., Bairoch, A., Wu, C. H.; Barker, W. C.; Boeckmann, B.; Ferro, S.; Gasteiger, E.; Huang, H.; Lopez, R.; Magrane, M.; Martin, M. J.; Natale, D. A.; O'Donovan, C.; Redaschi, N.; Yeh, L. S. *Nucleic Acids Res.* **2004**, *32*, D115−D119.

(32) http://www.matrixscience.com

(33) Anderson, N. L.; Anderson, N. G. *Mol. Cell Proteomics* **2002**, *1*, 845−867.

(34) Plasencia, M.; Valentine, S. J.; Liu, X.; Krishnan, M. and Clemmer, D. E., work in progress.

PR049877D